INTERNATIONAL JOURNAL OF HYDROGEN ENERGY XXX (2018) 1–12

Available online at www.sciencedirect.com

ScienceDirect

journal homepage: www.elsevier.com/locate/he

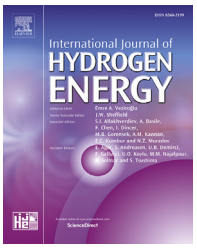

# Nickel-cobalt-oxide cathodes for hydrogen production by water electrolysis in acidic and alkaline media

*Abraham Gomez Vidales*[*], *Kanghoon Choi*, *Sasha Omanovic*

*Department of Chemical Engineering, McGill University, 3610 University St., Montreal, Quebec, H3A 0C5, Canada*

ARTICLE INFO

*Article history:*
Received 4 March 2018
Received in revised form
7 May 2018
Accepted 13 May 2018
Available online xxx

*Keywords:*
Hydrogen
Water electrolysis
Cobalt
Nickel
Metal oxides
Cathodes

ABSTRACT

Mixed Ni–Co-oxide cathodes of various compositions were fabricated by a thermal-decomposition method and used as electrocatalysts for hydrogen production by water electrolysis in acidic and alkaline media. The oxide electrodes were found to be of a semi-crystalline structure, yielding the surface morphology characterized by a surface roughness factor going up to 25. Linear potentiodynamic and potentiostatic electrochemical measurements revealed that the Volmer reaction step controlled the kinetics of the hydrogen evolution on all the Ni–Co-oxide cathodes, and also on the pure metal Ni electrode (control). The $Ni_{0.2}Co_{0.8}$-oxide was identified as the best electrode material candidate among the investigated metal oxides, which was linked to the surface-area effect. However, its intrinsic activity was found to be lower than that of pure metallic Ni. Nevertheless, the $Ni_{0.2}Co_{0.8}$-oxide electrode showed a significantly higher electrocatalytic stability (fouling/deactivation tolerance) in comparison to metallic Ni.



## Introduction

The demand for novel renewable energy has been increasing over the past few years due to the rapid depletion of the traditional energy sources, such as fossil fuels [1]. Many research efforts have sought ways to reduce the dependency on fossil fuels by trying to find an alternative power source. Hydrogen, the most abundant element in the universe, is considered to be an excellent green energy source due to its minimal impact on the environment [2]. Despite its abundance, hydrogen is hardly found as a separate element. Instead, it is primarily found in combination with carbon in hydrocarbon compounds, and with oxygen in water [3].

Hydrogen ($H_2$) can be obtained by water electrolysis, where electrical current is applied to split water into its components (oxygen and hydrogen). Hydrogen obtained by water electrolysis is a clean energy carrier since it can produce energy in fuel cells (or by burning) without emitting carbon dioxide [4]. Unfortunately, water electrolysis is not yet cost-competitive to hydrocarbon reforming due to its high operational costs (electricity cost, electrode degradation). In the case of production of hydrogen by polymer-electrolyte-membrane (PEM) electrolyzers, the operational costs per amount of produced hydrogen are lower in terms of the electricity used, but the cost of the PEM technology is higher in comparison to the conventional alkaline electrolyzers. This is mainly a consequence of the use of expensive noble metals (platinum,

* *Corresponding author.*
E-mail address: abraham.gomezvidales@mail.mcgill.ca (A. Gomez Vidales).
https://doi.org/10.1016/j.ijhydene.2018.05.068

ruthenium, and iridium) as electrocatalyst (electrode) materials, which are required due to the high acidity of the electrolyte environment [5]. In addition, despite the use of noble metals, the long-term stability and activity of electrodes are still not satisfactory. On the other hand, in alkaline electrolyzers, nickel electrodes could be used because of a much milder electrolyte environment (high pH). However, neither currently-used nickel electrodes offer satisfactory performance, especially regarding the fouling susceptibility (deactivation of Ni cathodes by electrochemically deposited trace metals) and mechanical stability. Also, further decrease in the hydrogen evolution reaction (HER) overpotential is required to make this process feasible.

An ideal electrode for the HER should have characteristics such as low overpotential, large active surface area, physical and electrochemical stability, high fouling resistance, low-cost, ease of use, and excellent electrical conductivity [6]. In this context, extensive research has been performed on the development of new electrode materials for hydrogen production [5–17]. Ni-based alloys have been identified as suitable candidates for electrodes in the alkaline water electrolysis, and in particular, Ni–Co has been found to offer electrocatalytic activity comparable to that of noble metals [16,18–22].

Unfortunately, pure metallic Ni-based alloys suffer two significant drawbacks. First, they cannot operate in PEM water electrolyzers due to their poor corrosion stability in the acidic medium. Second, they are susceptible to deactivation by electrodeposition of metallic impurities presented in the electrolyte, and thus their long-term stability and activity are not satisfactory even in alkaline water electrolyzers [23]. In the search for new materials, certain metal oxide electrodes have demonstrated excellent performance in the hydrogen evolution reaction, but they have not been widely studied [6,23,24]. The most intriguing aspect of metal oxides is that they have the ability to remain active for HER even in the presence of metallic impurities [23]. Furthermore, oxide electrodes have been claimed to be stable in both acidic and alkaline environments [25]. Due to the unique features of the metal oxides, they have been recognized as promising cathode materials for the electrocatalysis of HER [26].

The purpose of this research was to develop and study mixed Ni–Co-oxide cathodes for hydrogen production by water electrolysis in both the acidic and alkaline media. The rationale for choosing Ni–Co-oxides was due to their availability, low-cost, and promising results obtained in previous research studies as pure (non-oxide) alloy cathodes for hydrogen evolution [5,23]. The objective of this study is to report the effects of electrode composition and electrolyte temperature on the electrocatalytic performance for the HER.

## Experimental procedure

### *Electrode preparation*

$Ni_xCo_{(1-x)}$-oxide coatings (x = 0, 0.2, 0.4, 0.6, 0.8, 1; where x is the molar fraction and refers to the content of Ni and Co in the precursor solution) were formed on a flat titanium substrate by employing a thermal-decomposition method. A titanium button-shaped plate of 1.27 cm in diameter (purity 99.2%, Alfa Aesar, USA), with a thickness of 0.2 cm was used as the substrate. A first step of the electrode preparation process was to wet-polish the titanium substrate using 600-grit SiC sandpaper. Next, the polished plate was rinsed thoroughly and sonicated for 30 min in deionized water (resistivity 18.2 MΩ cm) to remove polishing residues. Then, the plate was etched in a boiling solution of hydrochloric acid (37 wt%, Fisher Scientific, Canada) and deionized water (1:1 by volume) for 30 min. After etching, the plate was again thoroughly rinsed with deionized water, and dried in argon gas (MEGS Specialty Gases Inc., 99.998 wt% pure, Canada).

To coat the titanium plate, a 0.2 M precursor solution was prepared by dissolving the metal precursor salts in an equivolume mixture of 37 wt% hydrochloric acid and deionized water. $NiCl_2 \times 6H_2O$ (purity 99.9%, Sigma-Aldrich, Canada), and $Co(NO_3)_2 \times 6H_2O$ (purity 99.7%, Acros Organics, Canada) were used as a source of nickel and cobalt, respectively. The coating solution was applied uniformly to the titanium substrate with a paintbrush (only one side of the titanium plate was coated with the precursor solution). After applying the first layer, the sample was placed in an oven at 383 K for five minutes to vaporize the solvent, followed by annealing the sample at 773 K in an air-natural-convection furnace for fifteen minutes. Next, the sample was removed from the furnace and allowed to cool for ten minutes, before another coating was applied. This same procedure was repeated six times to form a six-layered coating on the titanium substrate. Lastly, the sample was annealed in the furnace at 773 K for one hour to complete the oxidation of the coating to produce the $Ni_xCo_{(1-x)}$-oxides.

### *Electrochemical and surface/chemical composition characterization*

The electrochemical characterization of electrodes towards hydrogen evolution reaction was investigated using a three-electrode cell, at 293 ± 2 K and atmospheric pressure. The working electrode (WE) was at the bottom of the cell, fitted between a steel plate (to provide electrical contact) and the Teflon base of the cell containing an opening to the electrolyte. The geometrical area of the electrode exposed to the electrolyte solution was 0.68 $cm^2$. The counter electrode (CE), a graphite rod, was placed inside a glass tube plugged with a glass frit (Ace Glass Inc., USA) which prevented $O_2$ gas produced at the CE (anode) to migrate towards the WE and get reduced, thus interfering with the HER. A saturated calomel electrode (SCE) (Accumet electrode, Fisher Scientific, USA) was used as the reference electrode (RE). To maintain an oxygen-free electrolyte solution, the solution was purged by argon gas for 30 min before electrochemical measurements and continued to be purged during the measurements. In order to characterize the electrochemical behavior of the coatings, linear Tafel polarization (LTP), chronoamperometry (CA), chronopotentiometry (CP) measurements were performed using an Autolab PGSTAT30 potentiostat/galvanostat with NOVA software (v. 2.1; Metrohm, the Netherlands). Electrochemical measurements were done using two different electrolytes: 0.5 M $H_2SO_4$ (pH = 0.25) for the acidic

Please cite this article in press as: Gomez Vidales A, et al., Nickel-cobalt-oxide cathodes for hydrogen production by water electrolysis in acidic and alkaline media, International Journal of Hydrogen Energy (2018), https://doi.org/10.1016/j.ijhydene.2018.05.068

electrolysis (prepared using 96 wt% $H_2SO_4$, Fisher Scientific, Canada), and 1 M NaOH (pH = 14) for the alkaline electrolysis (prepared using 95 wt% purity NaOH crystals; Sigma-Aldrich, Canada).

The surface topography and chemical composition of the metal-oxide coatings were investigated using the scanning-electron-microscopy (SEM) and energy-dispersive X-ray spectroscopy (EDS) analysis (instrument: Hitachi SU-3500 Variable Pressure SEM/EDS detectors). The coatings' structural characterization was done employing the X-ray diffraction (XRD) analysis (instrument: Bruker D8 Discovery X-ray Diffractometer).

The electroactive surface area of the metal-oxide cathodes was determined by performing cyclic voltammetry (CV) and chronoamperometry (CA), using a solution of 1 mM HexRu(III) chloride (purity 98 wt%, Sigma-Aldrich, USA) in 0.1 M $KNO_3$ (purity 99 wt%, Fisher Scientific, Canada) as a redox probe [27–30]. For CV, a detailed description of this procedure can be found in our previous paper [31]. For CA, a current response at selected electrode potentials was recorded during the time of 15 s. Since the reduction of Ru(III) ion is a mass-transport controlled process, the recorded chronoamperogram follows the Cottrell equation $i = nFACD^{1/2}/(\pi t)^{1/2}$, where $n$ is the number of electrons appearing in half-reaction for the redox couple (one, in the current case), $F$ is the Faraday constant (96485 C $mol^{-1}$), $A$ is the electrochemically-active surface area ($cm^2$), $C$ is the concentration of the analyte in the bulk solution, HexRu(III) chloride (mol $cm^{-3}$), $D$ is the diffusion coefficient ($8.70 \times 10^{-6}$ $cm^2s^{-1}$ in the case of HexRu(III) in the used electrolyte), and $t$ is the time (s). The electrochemically-active area of the metal-oxide electrode was determined from the $i$ vs. $t^{-1/2}$ linear plot, and the values are combined with those obtained from CV measurements.

## Results and discussion

### Composition and structural characterization

Energy-dispersive spectroscopy verified the actual chemical composition of the coatings, and the results are presented in Table 1. From the results, it is seen that the actual Ni/Co ratio in the coating is very close to the nominal Ni/Co ratio (the ratio of Ni and Co in the precursor solutions). Furthermore, the EDS mapping of the coatings at several selected areas on the sample surface confirmed that the composition was uniform over the entire coating surface.

**Table 1 – Relative atomic percentage of Ni and Co in $Ni_xCo_{(1-x)}$-oxide coatings (excluding the contribution of oxygen in the coatings) obtained by EDS. These values refer to the measured concentration of Ni and Co on the surface of the coatings.**

| Element content, at. % | |
|---|---|
| Nominal | Experimental |
| NiOx | NiOx |
| $Ni_{0.8}Co_{0.2}Ox$ | $Ni_{0.74}Co_{0.26}Ox$ |
| $Ni_{0.6}Co_{0.4}Ox$ | $Ni_{0.56}Co_{0.44}Ox$ |
| $Ni_{0.4}Co_{0.6}Ox$ | $Ni_{0.42}Co_{0.58}Ox$ |
| $Ni_{0.2}Co_{0.8}Ox$ | $Ni_{0.12}Co_{0.88}Ox$ |
| CoOx | CoOx |

Another significant result emerged from the X-ray diffraction measurements. Fig. 1 shows the XRD patterns of all the samples. The spectra show that the coatings are mostly semi-crystalline. Distinct peaks characterized the diffraction pattern recorded on the pure Ni substrate: the peaks correspond, in increasing order of 2θ, to the (1 1 1), (2 0 0), and (2 2 0) reflections of the f.c.c. the structure of nickel (JCPDS card no. 4-0835) [32]; NiO peaks also appeared, and these were due to the oxidation of Ni in the air. For the NiO coating, the diffraction pattern obtained was identical to pure Ni but with higher intensity of peaks recorded at reflection planes of NiO (1 1 1) and (2 0 0) (JCPDS card no. 47-1049) [33]. Moreover, XRD detected the presence of $Ni_2O_3$ in the coating. Fig. 1 also reveals that Co-oxides present in each coating are characterized by some degree of amorphousness since they have relatively broader peaks than the Ni-oxides characteristic diffraction patterns. Two crystalline forms of Co-oxide are present in the coatings: CoO and $Co_3O_4$. Concerning the XRD pattern of Co-oxide coating, this matched well with the standard (JCPDS card no. 9-402). Based on the results of synthesis and characterization, it can be concluded that the stable phases of $Ni_xCo_{(1-x)}$-oxide using the proposed chemical route can be synthesized and that the degree of amorphousness augmented with the increase in cobalt content in the coatings.

### Morphology and electrochemical-active surface area of the electrodes

To examine the morphology of the coatings, a scanning electron microscopy technique was employed. The SEM images in Fig. 2 show differences in morphology of the investigated coatings. The corresponding particle size distribution was analyzed employing ImageJ software (v. 1.51, NIH, USA). The 600-grit polished Ni control sample (Fig. 2a) shows a surface of a certain degree of roughness. Instead, the Ni-oxide surface, Fig. 2b, shows a sponge-like structure. This structure displays a higher degree of roughness and a porous structure, relative to the nickel control sample.

The addition of Co into the coating significantly influences the morphology of the surface, as presented in Fig. 2c–f. Unlike the sponge-like structure of Ni-oxide, Co-containing $Ni_xCo_{(1-x)}$-oxide coatings display a granular structure. The $Ni_{0.8}Co_{0.2}$-oxide coating displays a lower degree of surface roughness and porosity than the pure Ni-oxide coating. Nevertheless, by increasing the Co content from 20% to 40%, the coating's porosity increases while the diameter of polygonal particles slightly increases from size ca. 0.8 ± 0.6 μm for the $Ni_{0.8}Co_{0.2}$-oxide coating to ca. 2.5 ± 0.9 μm for the $Ni_{0.6}Co_{0.4}$-oxide. By further increasing the Co content to 60%, the diameter (2.9 ± 1.1 μm) and the distribution of the particles remains similar to the 40% Co sample. For the $Ni_{0.2}Co_{0.8}$-oxide surface (Fig. 2f) and Co-oxide, the granular particle diameter slightly increased to 3.4 ± 1.5 μm and 3.1 ± 1.6 μm. Surprisingly, the pure Co-oxide coating (Fig. 2g) shows the morphology resembling that of the $Ni_xCo_{(1-x)}$-oxide coatings. This indicates that the Co-oxide present in these mixed metal

Please cite this article in press as: Gomez Vidales A, et al., Nickel-cobalt-oxide cathodes for hydrogen production by water electrolysis in acidic and alkaline media, International Journal of Hydrogen Energy (2018), https://doi.org/10.1016/j.ijhydene.2018.05.068

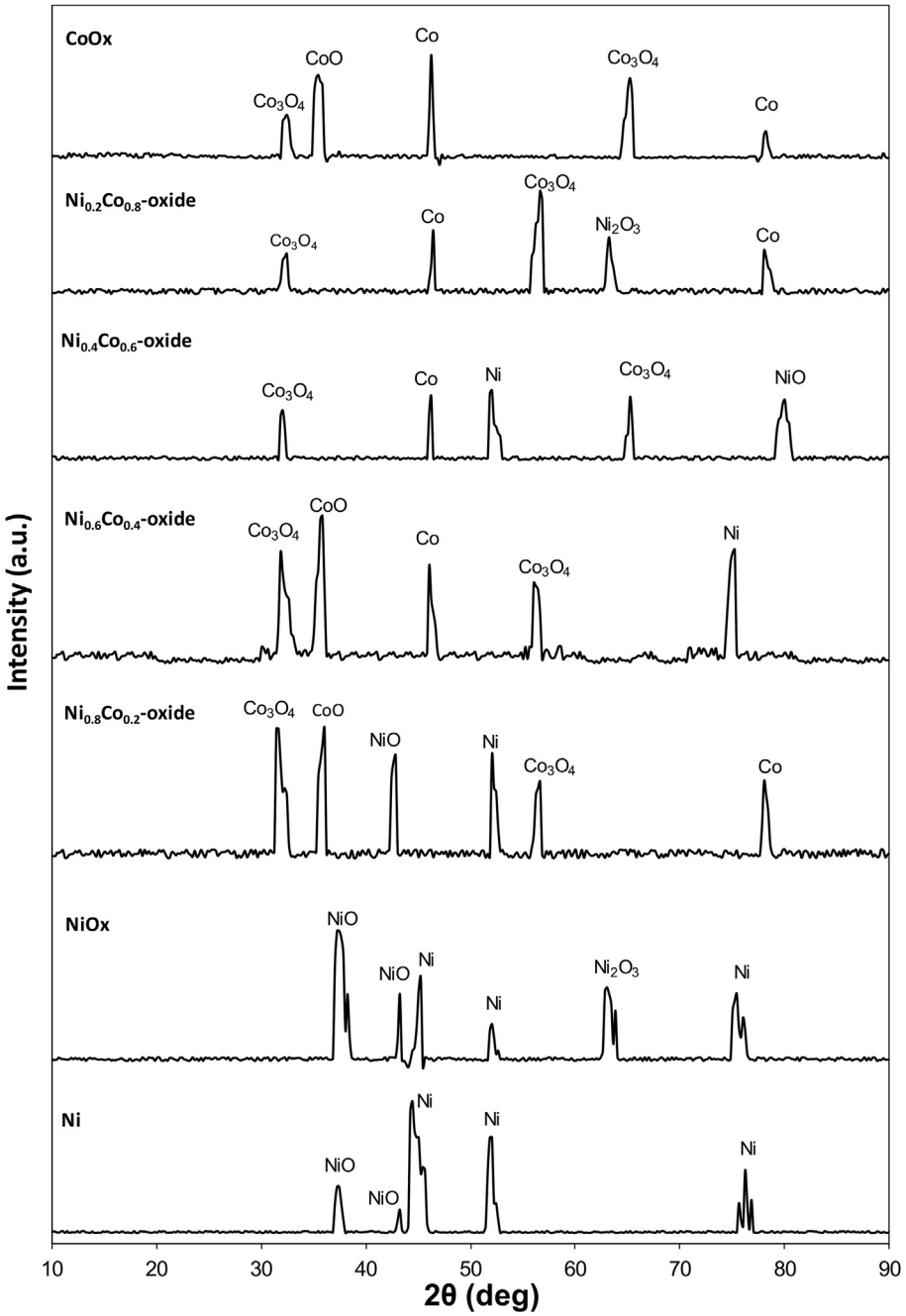


**Fig. 1 – X-ray diffraction spectra of $Ni_xCo_{(1-x)}$-oxide coatings deposited on a titanium substrate. Results for Ni-control sample are also presented for comparison.**

oxide coatings most-likely governs their morphology rather than the Ni-oxide, which is also supported by the difference between SEM images in Fig. 2 and those on Ni–Mo-oxide coatings published in our previous study [31].

Fig. 2 shows that the produced coatings display a varying degree of surface roughness and morphology, which implies differences in the size of the area of the coating exposed to the electrolyte, i.e., the electrochemically-active surface area size. To determine the electrochemically-active area of the surfaces, cyclic voltammetry and chronoamperometry in a ruthenium-complex solution was performed, as explained in the experimental section of the paper. The obtained values combining both techniques are presented in Table 2, together with the corresponding surface roughness factor.

Overall, in all the cases, the electrochemically-active surface areas were found to be considerably larger than the geometrical surface area of the electrocatalysts. Co-oxide electrode displayed the highest electrochemically active surface area, whereas the nickel control sample showed the lowest active area. Additionally, $Ni_{0.6}Co_{0.4}$-oxide, $Ni_{0.4}Co_{0.6}$-oxide, and $Ni_{0.2}Co_{0.8}$-oxide have surface areas which are very

Please cite this article in press as: Gomez Vidales A, et al., Nickel-cobalt-oxide cathodes for hydrogen production by water electrolysis in acidic and alkaline media, International Journal of Hydrogen Energy (2018), https://doi.org/10.1016/j.ijhydene.2018.05.068

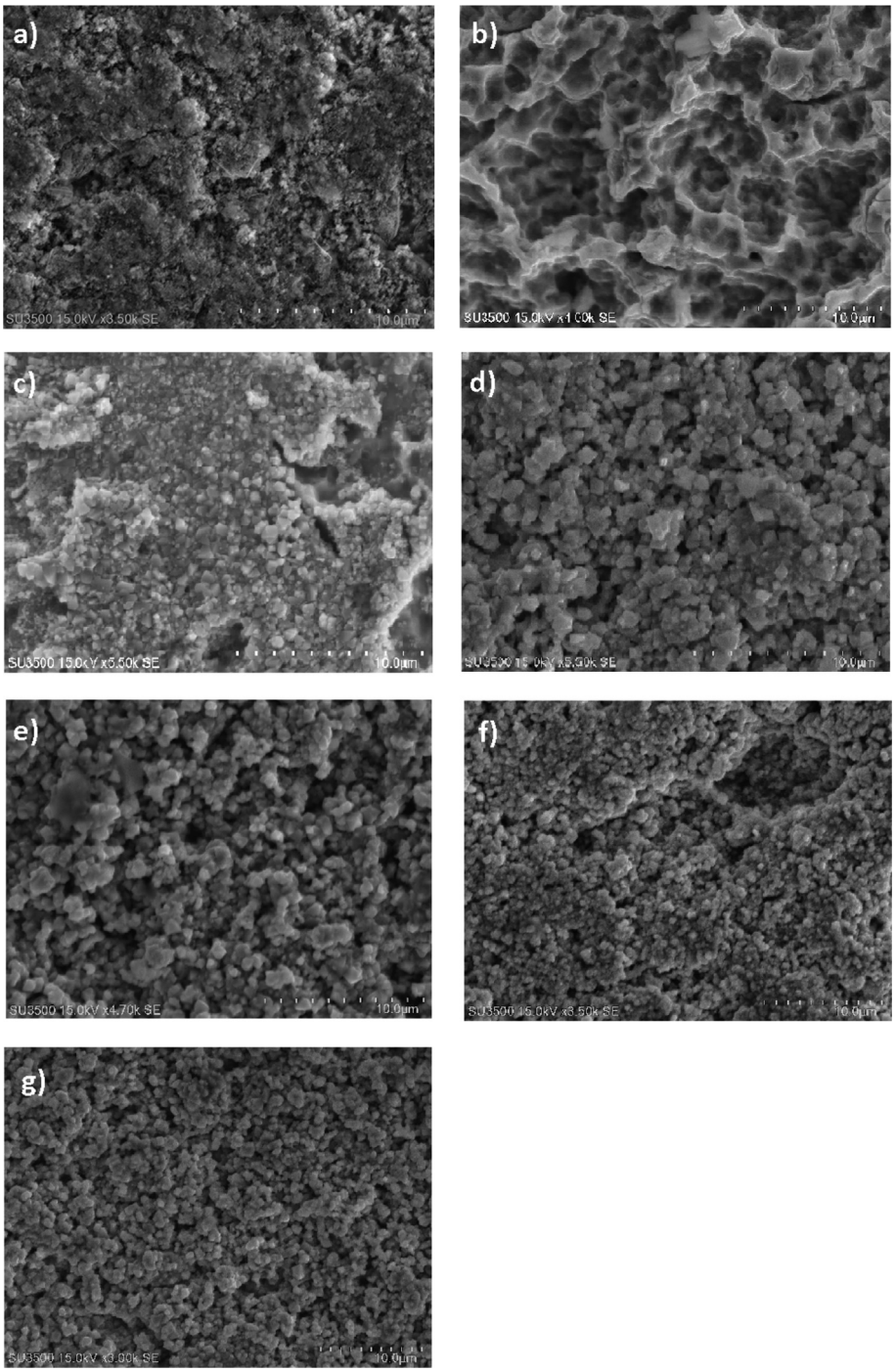


**Fig. 2 – SEM images showing a surface morphology of a) Ni metal plate (control sample), b) Ni-oxide, c) $Ni_{0.8}Co_{0.2}$-oxide, d) $Ni_{0.6}Co_{0.4}$-oxide, e) $Ni_{0.4}Co_{0.6}$-oxide, f) $Ni_{0.2}Co_{0.8}$-oxide, and g) Co-oxide coating. The overall scale length on the images is 10 μm.**

similar between them; this could be due to the similar diameter of the particles in these coatings. These results are consistent with the observations made based on the surface characterization of the coatings by SEM presented in Fig. 2. Also, the surface roughness values reported in Table 2 are close to those obtained for Ni–Mo-oxide coatings that are thermally deposited on Ti, although they go up to 52 for certain Ni–Mo-oxide compositions [31].

### *Electrocatalytic activity in the HER*

The electrocatalytic activity of the cathodes towards hydrogen evolution was investigated using linear Tafel polarization (LTP) and chronoamperometry (CA). Tafel polarization measurements were performed using two different electrolytes: 0.5 M $H_2SO_4$ and 1 M NaOH. Before electrochemical measurements, the electrode was pretreated for one hour at a

Please cite this article in press as: Gomez Vidales A, et al., Nickel-cobalt-oxide cathodes for hydrogen production by water electrolysis in acidic and alkaline media, International Journal of Hydrogen Energy (2018), https://doi.org/10.1016/j.ijhydene.2018.05.068

**Table 2 – True electrochemically-active surface area of Ni and $Ni_xCo_{(1-x)}$-oxide cathodes shown in Fig. 2 obtained by cyclic voltammetry and chronoamperometry. The geometric area is 0.68 $cm^2$.**

| Material | Electrochemically-active surface area ($cm^2$) | Surface roughness factor |
|---|---|---|
| Ni | 3.9 ± 0.6 | 5.7 |
| NiOx | 9.8 ± 2.6 | 14.4 |
| $Ni_{0.8}Co_{0.2}Ox$ | 6.2 ± 1.7 | 9.1 |
| $Ni_{0.6}Co_{0.4}Ox$ | 10.7 ± 2.7 | 15.7 |
| $Ni_{0.4}Co_{0.6}Ox$ | 8.5 ± 2.3 | 12.5 |
| $Ni_{0.2}Co_{0.8}Ox$ | 10.8 ± 3.1 | 15.9 |
| CoOx | 17.2 ± 3.5 | 25.3 |

potential of −1.60 V in 1 M NaOH and at −1.10 V in 0.5 M $H_2SO_4$, to ensure that all scans start with a conditioned surface. The polarization curves were corrected for the ohmic drop, where the electrolyte resistance value was obtained from EIS data (not shown here). CA measurements were done at selected potentials within the HER region for 300 s. From the CA measurements, the average current in the last 100 s was taken for further analysis.

Figs. 3 and 4 show sets of HER polarization curves recorded in 0.5 M $H_2SO_4$, and 1 M NaOH on all the investigated coatings, respectively. In these curves, the abscissa represents the overpotential, $\eta$ (V), which is the input driving force for the HER, while the current density, $j$ (A $cm^{-2}$), presented on the ordinate, represents the HER kinetics which is related to the amount of hydrogen produced through the Faraday law. The curves in Figs. 3 and 4 display the classical Tafelian behavior, with a linear region in the mid-potential range. The figures also evidence that there is a good agreement between the Tafel (semi-steady-state) and chronoamperometry (steady-state) curves. At high overpotentials, the curves start leveling into a plateau, possibly due to (i) a decrease in surface area of the electrode in contact with the electrolyte due to the attachment of produced $H_2$ bubbles to the surface, (ii) the formation of hydrides, and (iii) the local pH changes (increase) at the solid/liquid interface [20]. This effect is more prominent in the alkaline medium. As expected, when comparing the curves in the two electrolytes, the current densities obtained are, on average, higher in the acid medium than in the alkaline medium, since the acidic electrolyte has a higher concentration of hydrogen ions and therefore higher conductivity [34]. From the curves in Figs. 3 and 4, the cathodic Tafel slope, $b$ (mV $dec^{-1}$), the transfer coefficient, $\alpha$ (–), and the exchange current density, $j_0$ (μA $cm^{-2}$) were obtained, and the corresponding values are reported in Tables 3 and 4 for acidic and alkaline media, respectively. In general, a very good agreement between the Tafel and chronoamperometry sets of data was obtained, validating the values presented in both tables.

The HER is a two-step reaction, in which the first step is the formation of an adsorbed hydrogen atom intermediate, M-$H_{ads}$ (Volmer reaction). The second step is the generation of $H_2$ gas either through the reaction of an adsorbed hydrogen atom with the hydrogen ion (Heyrovsky reaction) or the chemical desorption by reaction of two hydrogen atoms adsorbed at neighbouring electrode sites (Tafel reaction). The corresponding Tafel slope values at 293 K for the previously mentioned reactions are 116, 40, and 30 mV $dec^{-1}$, respectively. These values govern the rate determining step of the HER mechanism [5]. The experimentally observed Tafel slope in Tables 3 and 4 range from 126 mV $dec^{-1}$ to 234 mV $dec^{-1}$ in the acidic medium and from 144 mV $dec^{-1}$ to 264 mV $dec^{-1}$ in the alkaline medium, indicating that the Volmer reaction is the rate-determining step for the HER on all the electrodes investigated in both electrolyte media. Lower values of Tafel slope are preferred since a smaller change in electrode overpotential results in a more significant increase in HER current, and thus higher hydrogen production rate [5]. In both acidic and alkaline media, only the $Ni_{0.2}Co_{0.8}$-oxide coating yielded average Tafel slope values lower than those on Ni (control sample), but the difference is not statistically significant. All other electrocatalysts have larger Tafel slopes, which could be due to the weaker electronic conductivity of the oxide coatings in comparison to pure Ni. Nonetheless, the Tafel slopes obtained for the $Ni_xCo_{(1-x)}$-oxide cathodes produced here are considerably lower than what has been reported on some other bimetallic-oxides [35] but are comparable to the values obtained on Ni–Mo-oxide coatings thermally deposited on Ti [31].

Another comparison parameter used to investigate the electrocatalytic activity of the prepared catalysts is the

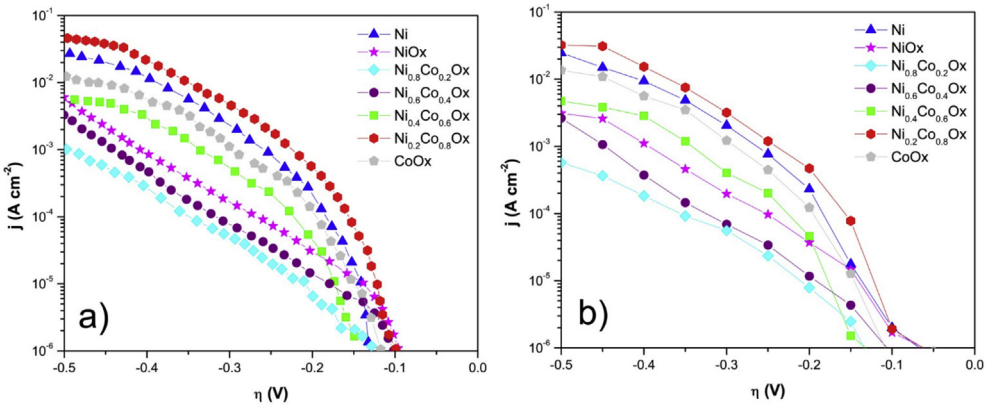


**Fig. 3 – Polarization curves recorded in 0.5 M $H_2SO_4$ on a Ni control sample and on $Ni_xCo_{(1-x)}$-oxide coatings by (a) LTP and b) CA. Temperature = 293 ± 2 K. Scan rate in LTP was 1 $mVs^{-1}$, and in both cases, the polarization was done from high to low overpotentials.**

Please cite this article in press as: Gomez Vidales A, et al., Nickel-cobalt-oxide cathodes for hydrogen production by water electrolysis in acidic and alkaline media, International Journal of Hydrogen Energy (2018), https://doi.org/10.1016/j.ijhydene.2018.05.068

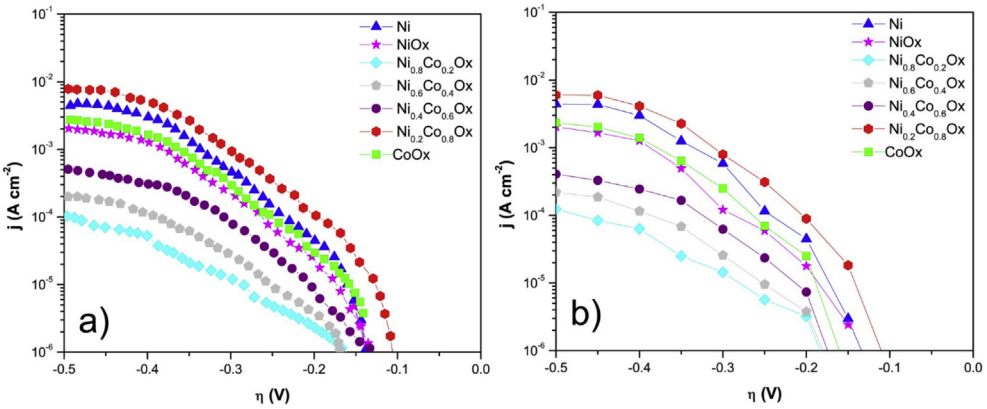


**Fig. 4 – Polarization curves recorded in 0.1 M NaOH on a Ni control sample and on $Ni_xCo_{(1-x)}$-oxide coatings by (a) LTP and b) CA. Temperature = 293 ± 2 K. Scan rate in LTP was 1 $mVs^{-1,}$ and in both cases, the polarization was done from high to low overpotentials.**

**Table 3 – Kinetic parameters (Tafel slope, transfer coefficient, and exchange current density) for the $Ni_xCo_{(1-x)}$-oxide coatings obtained in 0.5 M $H_2SO_4$ solution. Results for the Ni-control sample are also presented for comparison. Presented errors are standard deviations of the mean. Temperature = 293 ± 2.**

| Sample | *Tafel polarization data* | | | *Chronoamperometry data* | | |
|---|---|---|---|---|---|---|
| | $b$ (mV $dec^{-1}$) | $\alpha$ | $J_0$ (μA $cm^{-2}$) | $b$ (mV $dec^{-1}$) | $\alpha$ | $j_0$ (μA $cm^{-2}$) |
| Ni | 134 ± 9 | 0.44 ± 0.03 | 15.2 ± 3.21 | 142 ± 12 | 0.42 ± 0.06 | 10.2 ± 4.62 |
| NiOx | 173 ± 16 | 0.34 ± 0.05 | 1.82 ± 0.24 | 170 ± 19 | 0.32 ± 0.08 | 1.21 ± 0.44 |
| $Ni_{0.8}Co_{0.2}Ox$ | 223 ± 21 | 0.26 ± 0.02 | 0.21 ± 0.02 | 234 ± 26 | 0.24 ± 0.04 | 0.16 ± 0.05 |
| $Ni_{0.6}Co_{0.4}Ox$ | 214 ± 18 | 0.27 ± 0.04 | 0.47 ± 0.09 | 223 ± 22 | 0.25 ± 0.07 | 0.35 ± 0.08 |
| $Ni_{0.4}Co_{0.6}Ox$ | 162 ± 12 | 0.36 ± 0.08 | 1.53 ± 0.83 | 179 ± 14 | 0.34 ± 0.04 | 1.34 ± 0.71 |
| $Ni_{0.2}Co_{0.8}Ox$ | 126 ± 8 | 0.47 ± 0.07 | 25.3 ± 2.42 | 133 ± 13 | 0.45 ± 0.09 | 20.2 ± 3.82 |
| CoOx | 154 ± 11 | 0.38 ± 0.06 | 3.12 ± 0.91 | 165 ± 15 | 0.36 ± 0.05 | 2.71 ± 0.72 |

**Table 4 – HER kinetic parameters (Tafel slope, transfer coefficient, and exchange current density) for the $Ni_xCo_{(1-x)}$-oxide coatings obtained in 1 M NaOH solution. Results for the Ni-control sample are also presented for comparison. Presented errors are standard deviations of the mean. Temperature = 293 ± 2.**

| Sample | *Tafel polarization data* | | | *Chronoamperometry data* | | |
|---|---|---|---|---|---|---|
| | $b$ (mV $dec^{-1}$) | $\alpha$ | $j_0$ (μA $cm^{-2}$) | $b$ (mV $dec^{-1}$) | $\alpha$ | $j_0$ (μA $cm^{-2}$) |
| Ni | 156 ± 10 | 0.38 ± 0.04 | 0.96 ± 0.17 | 163 ± 18 | 0.36 ± 0.04 | 0.73 ± 0.24 |
| NiOx | 176 ± 12 | 0.33 ± 0.08 | 0.64 ± 0.13 | 186 ± 21 | 0.31 ± 0.08 | 0.42 ± 0.19 |
| $Ni_{0.8}Co_{0.2}Ox$ | 234 ± 14 | 0.25 ± 0.03 | 0.07 ± 0.03 | 264 ± 22 | 0.23 ± 0.03 | 0.02 ± 0.02 |
| $Ni_{0.6}Co_{0.4}Ox$ | 224 ± 18 | 0.26 ± 0.05 | 0.08 ± 0.02 | 241 ± 24 | 0.24 ± 0.05 | 0.06 ± 0.01 |
| $Ni_{0.4}Co_{0.6}Ox$ | 203 ± 13 | 0.29 ± 0.02 | 0.11 ± 0.06 | 212 ± 18 | 0.27 ± 0.02 | 0.14 ± 0.06 |
| $Ni_{0.2}Co_{0.8}Ox$ | 144 ± 9 | 0.41 ± 0.09 | 3.63 ± 1.12 | 153 ± 12 | 0.39 ± 0.09 | 2.91 ± 1.12 |
| CoOx | 182 ± 12 | 0.32 ± 0.06 | 0.35 ± 0.08 | 202 ± 19 | 0.30 ± 0.06 | 0.21 ± 0.08 |

transfer coefficient $\alpha$, derived from the Tafel slope: $b = 2.303\ RT/(\alpha F)$ where $R$ is the gas constant (8.314 $JK^{-1}$ $mol^{-1}$), $T$ is temperature (K), and $F$ is the Faraday constant 96485 C $mol^{-1}$. A higher transfer coefficient value indicates better electrocatalytic activity [36]. Similarly, to the Tafel slope values, only the $Ni_{0.2}Co_{0.8}$-oxide catalyst yielded an average transfer coefficient value that is higher than that of the Ni control sample, but again, the difference is not statistically significant (Tables 3 and 4). The same occurs when the exchange current density values are compared. With respect to the latter, the exchange current density value obtained for Ni agrees with the value presented on the HER volcano plot [37]. The value recorded on $Ni_{0.2}Co_{0.8}$-oxide is higher, but it is still ca. 1.5–2 orders of magnitude lower than the value obtained on noble metals (Pt, Ir, Ru).

Although the kinetic parameters in Tables 3 and 4 offer information on the relative performance of the coatings in the HER, a more practical way of evaluating them is by comparing the HER current (amount of $H_2$ evolved) at a fixed overpotential [5]. Fig. 5 displays the current density values for HER recorded in both the acidic and alkaline media at an overpotential of −300 mV, normalized to the geometrical area of the electrode (the values were obtained from the curves in Figs. 3 and 4). It is evident that the highest apparent electrocatalytic activity is obtained for the $Ni_{0.2}Co_{0.8}$-oxide electrode in both electrolyte media, which is in accordance with the

Please cite this article in press as: Gomez Vidales A, et al., Nickel-cobalt-oxide cathodes for hydrogen production by water electrolysis in acidic and alkaline media, International Journal of Hydrogen Energy (2018), https://doi.org/10.1016/j.ijhydene.2018.05.068

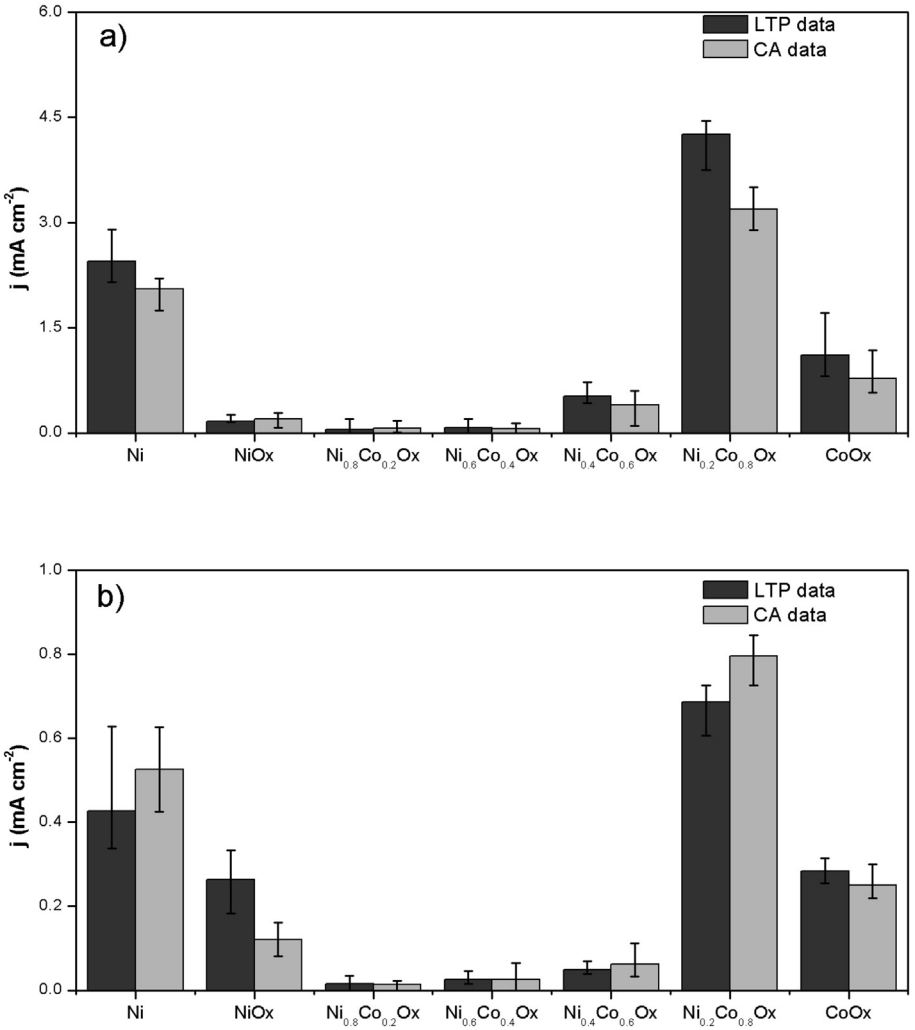


**Fig. 5 – Comparison of the electrocatalytic activity of the investigated electrode materials in the HER in terms of current density expressed per geometric area of the electrode and measured at an overpotential of −300 mV in a) 0.5 M $H_2SO_4$ and b) 1 M NaOH. Temperature = 293 ± 2 K.**

kinetic parameters in Tables 3 and 4. The other $Ni_xCo_{(1-x)}$-oxide coatings are significantly inferior to the control electrode in the acidic medium, while in the alkaline electrolyte pure Ni-oxide and Co-oxide coatings show the HER electrocatalytic activity slightly lower than that of the control surface.

The information obtained from the polarization data demonstrates that the $Ni_{0.2}Co_{0.8}$-oxide catalyst shows superior apparent electrocatalytic activity over pure Ni in both acidic and alkaline media. However, the data in Fig. 5 are normalized with respect to the geometrical area of the electrode, which does not enable us to evaluate the intrinsic electrocatalytic activity of the metal-oxide electrodes in the HER. Consequently, in order to assess which of the electrocatalysts is intrinsically the best material for the HER, the results presented in Fig. 5 were normalized with respect to the true electrochemically-active surface area of the electrocatalyst (Fig. 6), the latter obtained from average of the CV and CA measurements in the HexRu(III) chloride-containing solution.

As shown in Fig. 6, the control Ni sample has the highest intrinsic catalytic activity in both media, followed by $Ni_{0.2}Co_{0.8}$-oxide. This observation demonstrates that the higher electrocatalytic activity of the $Ni_{0.2}Co_{0.8}$-oxide coating seen in Fig. 5 is due to the surface-area effect. Nevertheless, one should note that the control Ni surface cannot be used in PEM-type electrolyzers due to poor corrosion stability of Ni in the acidic medium. In addition, metal-oxide electrodes are significantly less susceptible to fouling (deactivation) than pure metal electrodes. Hence, among the investigated electrodes (including the control Ni surface), the $Ni_{0.2}Co_{0.8}$-oxide electrode seems, from the practical point of view, to be the best surface for the HER in the acidic medium, but also in alkaline media that contain traces of heavy metals. When comparing to Ni–Mo-oxide coatings, the Ni–Co-oxide coatings display lower intrinsic catalytic activity [31]; the $Ni_{0.2}Co_{0.8}$-oxide coating (Fig. 6) yields ca. 41% activity of the best Ni–Mo-oxide composition ($Ni_{0.8}Mo_{0.2}$-oxide) in the acidic medium, and 24% of that one in the alkaline medium. It would be too speculative to try to explain the difference only on the

Please cite this article in press as: Gomez Vidales A, et al., Nickel-cobalt-oxide cathodes for hydrogen production by water electrolysis in acidic and alkaline media, International Journal of Hydrogen Energy (2018), https://doi.org/10.1016/j.ijhydene.2018.05.068

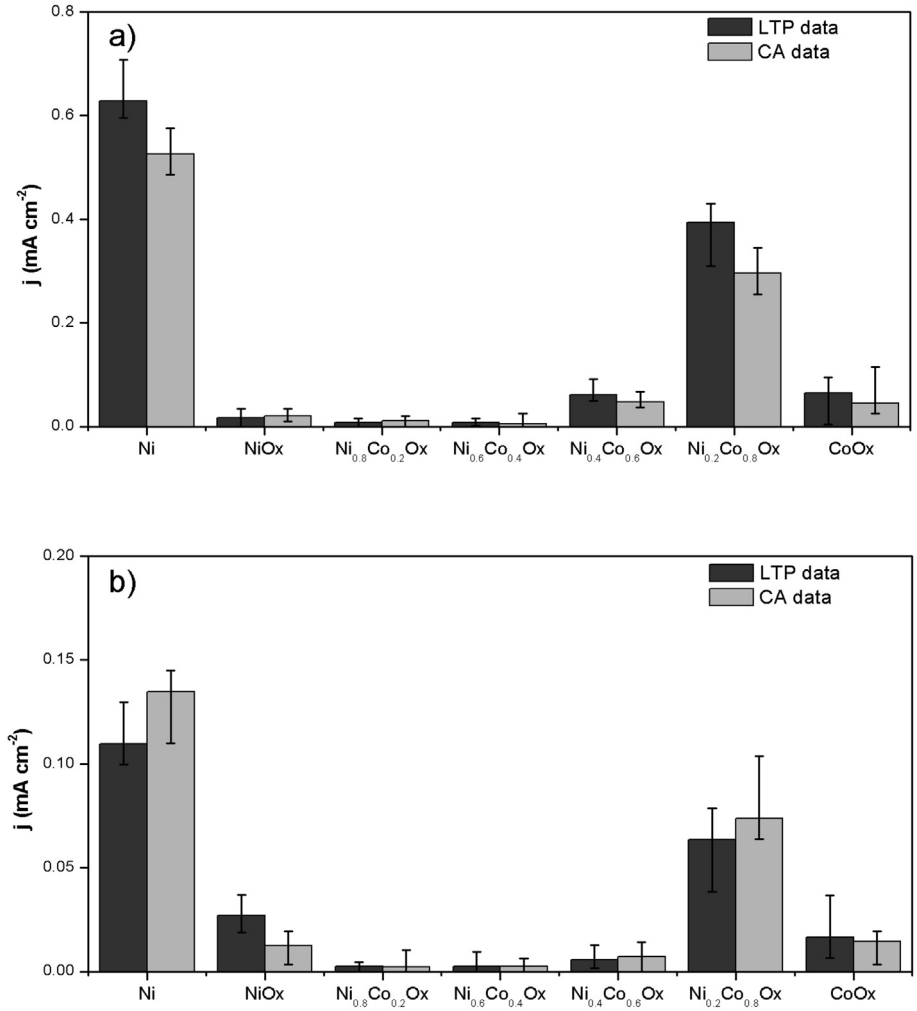


**Fig. 6 – Comparison of the electrocatalytic activity of the investigated electrode materials in the HER in terms of current density expressed per true electrochemically-active area of the electrode and measured at an overpotential of −300 mV in a) 0.5 M $H_2SO_4$ and b) 1 M NaOH. Temperature = 293 ± 2 K.**

basis of chemical composition, i.e., the influence of Mo *vs*. Co, since a range of other factors determine the HER activity of the two materials (electronic structure, surface energy, extent/shape/distribution of nano-pores in the material, to name a few).

### *Long-term stability of the electrodes*

The electrocatalytic stability of selected electrodes used in this work was tested in aggressive 0.5 $H_2SO_4$ by running linear Tafel polarization (LTP) and chronopotentiometry (CP) measurements consecutively in the following order: LTP on freshly-prepared electrodes, CP at −0.5 A $cm^{-2}$ for 72 h (note that this current is higher by an order of magnitude than the maximum current in Fig. 3), and LTP again on the previously used electrodes. Then, the current at −300 mV was determined from the LTP curves before and after 72 h; the corresponding percentage of electrode activity is presented in Fig. 7. A significant decrease (ca. by 45%) in electrocatalytic activity recorded for the Ni control sample can be observed. Given that the *bulk* Ni metal was used as the cathode in these

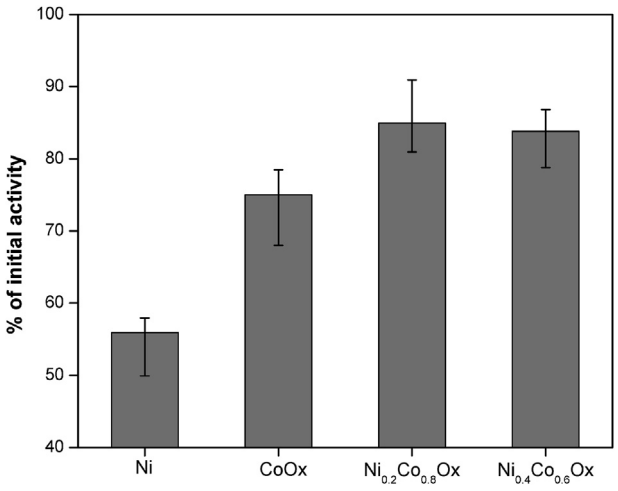


**Fig. 7 – Percentage of electrode deactivation of selected electrodes in the HER measured at an overpotential of −300 mV in 0.5 M $H_2SO_4$ after 72 h of electrolysis at 0.5 A $cm^{-2}$.**

Please cite this article in press as: Gomez Vidales A, et al., Nickel-cobalt-oxide cathodes for hydrogen production by water electrolysis in acidic and alkaline media, International Journal of Hydrogen Energy (2018), https://doi.org/10.1016/j.ijhydene.2018.05.068

measurements (thus, the anodic leveling of the surface, i.e., a decrease in surface roughness, can be excluded), this indicates that the decline in electrocatalytic activity with time could be due to the fouling of the Ni electrode surface by metal impurities present in traces in the electrolyte (the source of these impurities is the 96 wt% stock $H_2SO_4$ used to prepare the electrolyte). On the other hand, the oxide electrodes showed a much smaller decrease in electrocatalytic activity, indicating that they are significantly more fouling/deactivation tolerant in comparison to metallic Ni. Thus, the HER current recorded on the most (apparently) active $Ni_{0.2}Co_{0.8}$-oxide electrode decreased by ca. 15%, while for the other two oxide electrodes the decrease is not statistically significant. Nonetheless, a more detailed analysis of the coatings, over a more extended period is recommended to evaluate both the kinetics and mechanism of deactivation, which is outside of the scope of current work.

### *Temperature effect and activation energy*

To evaluate the effect of temperature on the kinetics of the HER on the $Ni_{0.2}Co_{0.8}$-oxide electrode, steady-state polarization curves for the HER in 0.5 M $H_2SO_4$ were recorded in the temperature range from 293 K to 323 K (see Fig. 8). As expected, with an increase in temperature, the HER activity is enhanced.

In order to test whether the HER kinetics on $Ni_{0.2}Co_{0.8}$-oxide follows the Arrhenius type of behavior, the data from Fig. 8 were used to estimate the linearity w.r. to the Arrhenius equation: $ln(j\eta_{=const}) = -E_a/RT + ln(A)$, where $E_a$ (J mol$^{-1}$) represents the apparent activation energy for the HER, and A (A cm$^{-2}$) is the pre-exponential factor. Fig. 9 shows the corresponding behavior at three selected HER overpotentials. Evidently, the HER kinetics on $Ni_{0.2}Co_{0.8}$-oxide indeed follows the Arrhenius law. From the slope of the lines, the corresponding apparent activation energy was calculated at each potential, and the following values were obtained: 39.2, 35.3, 31.9 kJ mol$^{-1}$ at −200, −300 and −400 mV, respectively. As it can be seen, the activation energy is a potential-dependent

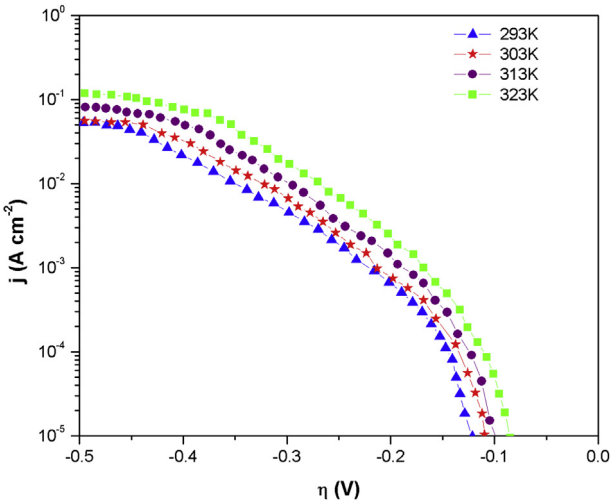


**Fig. 8 – Polarization curves recorded in 0.5 M $H_2SO_4$ on a $Ni_{0.2}Co_{0.8}$-oxide electrode at different temperatures.**

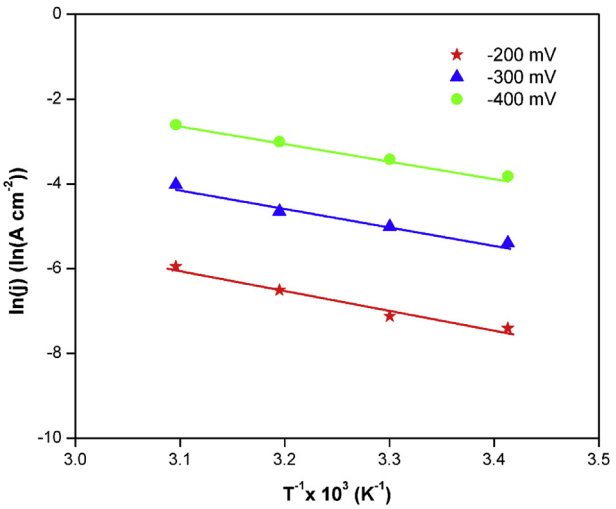


**Fig. 9 – Arrhenius-type semi-logarithmic dependence of current density on inverse temperature obtained at several selected overpotentials from the polarization curves presented in Fig. 8.**

value [38], and if the HER mechanism remains constant within a given potential range, with an increase in overpotential a linear decrease in activation energy can be expected from the theory of electrochemical kinetics [39]. Therefore, in order to make a proper comparison, the corresponding activation energy at zero overpotential, $E_{a,rev}$, was calculated from the $E_a$ *vs.* $\eta$ dependence (plot not shown here; $R_2 = 0.998$). The value obtained is $E_{a,rev} = 46.4$ kJ mol$^{-1}$, which is in the range of values reported for nickel and nickel metal (non-oxide) alloys [12,15]. Savadogo et al. [40] obtained values ranging from 36 to 56 kJ mol$^{-1}$ on Pt–Co supported on carbon, while Damian et al. [15] reported values of 44–73 kJ mol$^{-1}$ on Ni–Mo cathodes electrodeposited in a three-dimensional polyaniline matrix.

## Conclusion

The use of $Ni_xCo_{(1-x)}$-oxide electrode coatings of various composition produced by a thermal-decomposition method was investigated in the hydrogen evolution reaction in acidic and alkaline media. The oxide electrodes were found to be of a semi-crystalline structure, yielding the surface morphology characterized by relatively high surface roughness factor (up to 25). The potentiodynamic and potentiostatic measurements were used to determine the mechanism and kinetics of the HER. From this, it was shown that the kinetics of the HER on $Ni_xCo_{1-x}$-oxide cathodes was controlled by the Volmer reaction step as the rate-determining step, i.e., by the electrochemical adsorption of hydrogen. $Ni_{0.2}Co_{0.8}$-oxide was identified as the most apparently-active coating among the investigated materials, as it yielded the highest apparent electrocatalytic activity (normalized with respect to the geometric surface area) in both the acidic and alkaline media. However, when the activity was evaluated taking into account the electrochemically-active area, the control sample (Ni) showed the highest intrinsic electrocatalytic activity.

Please cite this article in press as: Gomez Vidales A, et al., Nickel-cobalt-oxide cathodes for hydrogen production by water electrolysis in acidic and alkaline media, International Journal of Hydrogen Energy (2018), https://doi.org/10.1016/j.ijhydene.2018.05.068

Nevertheless, we still suggest $Ni_{0.2}Co_{0.8}$-oxide be used as the cathode since (i) pure Ni cannot be used in PEM-type electrolyzers due to poor corrosion stability of Ni in the acidic medium, (ii) pure Ni is prone to fouling even in alkaline electrolyzers due to electrodeposition of impurities present in the electrolyte in traces, and since (iii) metal-oxide electrodes are significantly less susceptible to fouling (deactivation) by impurities (e.g., heavy metals) present in electrolytes used in alkaline hydrogen electrolyzers. Nonetheless, for PEM-type electrolyzers, it is recommended to produce $Ni_{0.2}Co_{0.8}$-oxide in the form of nanoparticles, which could potentially increase the electrode electrical conductivity and also their intrinsic activity due to the increase in surface energy.

## Acknowledgements

Financial support from the McGill University through the McGill Engineering Doctoral Award (MEDA) program, the National Council of Science and Technology of Mexico (CONACYT), and the Natural Sciences and Engineering Council (NSERC) of Canada is gratefully acknowledged.

## REFERENCES

[1] Edwards PP, Kuznetsov VL, David WI, Brandon NP. Hydrogen and fuel cells: towards a sustainable energy future. Energy Pol 2008;36:4356–62.
[2] Hijikata T. Research and development of international clean energy network using hydrogen energy (WE-NET). Int J Hydrogen Energy 2002;27:115–29.
[3] Momirlan M, Veziroglu TN. The properties of hydrogen as fuel tomorrow in sustainable energy system for a cleaner planet. Int J Hydrogen Energy 2005;30:795–802.
[4] De Souza RF, Padilha JC, Gonçalves RS, De Souza MO, Rault-Berthelot J. Electrochemical hydrogen production from water electrolysis using ionic liquid as electrolytes: towards the best device. J Power Sources 2007;164:792–8.
[5] Navarro-Flores E, Chong Z, Omanovic S. Characterization of Ni, NiMo, NiW and NiFe electroactive coatings as electrocatalysts for hydrogen evolution in an acidic medium. J Mol Catal A Chem 2005;226:179–97.
[6] Shibli S, Sebeelamol J. Development of Fe 2 O 3–TiO 2 mixed oxide incorporated Ni–P coating for electrocatalytic hydrogen evolution reaction. Int J Hydrogen Energy 2013;38:2271–82.
[7] Jaksic MM. Hypo–hyper-d-electronic interactive nature of interionic synergism in catalysis and electrocatalysis for hydrogen reactions. Int J Hydrogen Energy 2001;26:559–78.
[8] Kirk D, Thorpe S, Suzuki H. Ni-base amorphous alloys as electrocatalysts for alkaline water electrolysis. Int J Hydrogen Energy 1997;22:493–500.
[9] Zeng K, Zhang D. Recent progress in alkaline water electrolysis for hydrogen production and applications. Prog Energy Combust Sci 2010;36:307–26.
[10] Raj IA. Nickel-based, binary-composite electrocatalysts for the cathodes in the energy-efficient industrial production of hydrogen from alkaline-water electrolytic cells. J Mater Sci 1993;28:4375–82.
[11] Ezaki H, Morinaga M, Watanabe S, Saito J. Hydrogen overpotential for intermetallic compounds, TiAl, FeAl and NiAl, containing 3d transition metals. Electrochim Acta 1994;39:1769–73.
[12] Kawashima A, Akiyama E, Habazaki H, Hashimoto K. Characterization of sputter-deposited Ni-Mo and Ni-W alloy electrocatalysts for hydrogen evolution in alkaline solution. Mater Sci Eng A 1997;226:905–9.
[13] Jakšić J, Vojnović M, Krstajić N. Kinetic analysis of hydrogen evolution at Ni–Mo alloy electrodes. Electrochim Acta 2000;45:4151–8.
[14] Highfield J, Oguro K, Grushko B. Raney multi-metallic electrodes from regular crystalline and quasi-crystalline precursors: I. Cu-stabilized Ni/Mo cathodes for hydrogen evolution in acid. Electrochim Acta 2001;47:465–81.
[15] Damian A, Omanovic S. Ni and Ni Mo hydrogen evolution electrocatalysts electrodeposited in a polyaniline matrix. J Power Sources 2006;158:464–76.
[16] Rosalbino F, Delsante S, Borzone G, Angelini E. Electrocatalytic behaviour of Co–Ni–R (R= Rare earth metal) crystalline alloys as electrode materials for hydrogen evolution reaction in alkaline medium. Int J Hydrogen Energy 2008;33:6696–703.
[17] McArthur M, Jorge L, Coulombe S, Omanovic S. Synthesis and characterization of 3D Ni nanoparticle/carbon nanotube cathodes for hydrogen evolution in alkaline electrolyte. J Power Sources 2014;266:365–73.
[18] Krstajic N, Trasatti S. Cathodic behaviour of RuO2-doped Ni/Co3O4 electrodes in alkaline solutions: hydrogen evolution. J Appl Electrochem 1998;28:1291–7.
[19] Trasatti S. Electrocatalysis: understanding the success of DSA®. Electrochim Acta 2000;45:2377–85.
[20] Cao B, Veith GM, Neuefeind JC, Adzic RR, Khalifah PG. Mixed close-packed cobalt molybdenum nitrides as non-noble metal electrocatalysts for the hydrogen evolution reaction. J Am Chem Soc 2013;135:19186–92.
[21] Zhao Z, Wu H, He H, Xu X, Jin Y. A high-performance binary Ni–Co hydroxide-based water oxidation electrode with three-dimensional coaxial nanotube array structure. Adv Funct Mater 2014;24:4698–705.
[22] Yan X, Tian L, Atkins S, Liu Y, Murowchick J, Chen X. Converting CoMoO4 into CoO/MoO x for overall water splitting by hydrogenation. ACS Sustainable Chem Eng 2016;4:3743–9.
[23] Trasatti S. Hydrogen evolution on oxide electrodes. Modern chlor-alkali technology. Springer; 1992. p. 281–94.
[24] Tavares A, Trasatti S. Ni+ RuO 2 co-deposited electrodes for hydrogen evolution. Electrochim Acta 2000;45:4195–202.
[25] Blouin M, Guay D. Activation of ruthenium oxide, iridium oxide, and mixed RuxIr1− x oxide electrodes during cathodic polarization and hydrogen evolution. J Electrochem Soc 1997;144:573–81.
[26] Li YH, Liu PF, Pan LF, Wang HF, Yang ZZ, Zheng LR, et al. Local atomic structure modulations activate metal oxide as electrocatalyst for hydrogen evolution in acidic water. Nat Commun 2015;6:8064.
[27] Wang Y, Limon-Petersen JG, Compton RG. Measurement of the diffusion coefficients of [Ru (NH 3) 6] 3+ and [Ru (NH 3) 6] 2+ in aqueous solution using microelectrode double potential step chronoamperometry. J Electroanal Chem 2011;652:13–7.
[28] Limon-Petersen JG, Han JT, Rees NV, Dickinson EJF, Streeter I, Compton RG. Quantitative voltammetry in weakly supported media. Chronoamperometric studies on diverse one electron redox couples containing various charged species: dissecting diffusional and migrational contributions and assessing the breakdown of electroneutrality. J Phys Chem C 2010;114:2227–36.
[29] Sreenivas G, Ang SS, Fritsch I, Brown WD, Gerhardt GA, Woodward DJ. Fabrication and characterization of

sputtered-carbon microelectrode arrays. Anal Chem 1996;68:1858–64.
[30] Keeley GP, O'Neill A, McEvoy N, Peltekis N, Coleman JN, Duesberg GS. Electrochemical ascorbic acid sensor based on DMF-exfoliated graphene. J Mater Chem 2010;20:7864–9.
[31] Gomez Vidales A, Omanovic S. Evaluation of nickel-molybdenum-oxides as cathodes for hydrogen evolution by water electrolysis in acidic, alkaline, and neutral media. Electrochim Acta 2018;262:115–23.
[32] Wen X, Chen X, Tian N, Gong J, Liu J, Rümmeli MH, et al. Nanosized carbon black combined with Ni2O3 as "universal" catalysts for synergistically catalyzing carbonization of polyolefin wastes to synthesize carbon nanotubes and application for supercapacitors. Environ Sci Technol 2014;48:4048–55.
[33] Richardson JT, Scates R, Twigg MV. X-ray diffraction study of nickel oxide reduction by hydrogen. Appl Catal A Gen 2003;246:137–50.
[34] Zheng Y, Jiao Y, Jaroniec M, Qiao SZ. Advancing the electrochemistry of the hydrogen-evolution reaction through combining experiment and theory. Angew Chem Int Ed 2015;54:52–65.
[35] Metikoš-Huković M, Jukić A. Correlation of electronic structure and catalytic activity of Zr–Ni amorphous alloys for the hydrogen evolution reaction. Electrochim Acta 2000;45:4159–70.
[36] Zeng M, Li Y. Recent advances in heterogeneous electrocatalysts for the hydrogen evolution reaction. J Mater Chem A 2015;3:14942–62.
[37] Trasatti S. Work function, electronegativity, and electrochemical behaviour of metals: III. Electrolytic hydrogen evolution in acid solutions. J Electroanal Chem Interfacial Electrochem 1972;39:163–84.
[38] Bagotsky VS. Fundamentals of electrochemistry. John Wiley & Sons; 2005.
[39] Prentice G. Electrochemical engineering principles. 1991.
[40] Savadogo O, Ndzebet E. Influence of SiW 12 O 40 4– on the electrocatalytic behaviour of Pt–Co alloy supported on carbon for water electrolysis in 3 M KOH aqueous solution. Int J Hydrogen Energy 2001;26:213–8.

Please cite this article in press as: Gomez Vidales A, et al., Nickel-cobalt-oxide cathodes for hydrogen production by water electrolysis in acidic and alkaline media, International Journal of Hydrogen Energy (2018), https://doi.org/10.1016/j.ijhydene.2018.05.068